Effect of Substitution of Pb for Mg on the Photovoltaic Properties of Methyl-ammonium Lead Iodide Perovskites

César Tablero Crespo
Instituto de Energía Solar, E.T.S.I. de Telecomunicación,
Universidad Politécnica de Madrid,
Ciudad Universitaria s/n, 28040 Madrid, SPAIN.
e-mail: ctablero@etsit.upm.es

Abstract

To know if Pb can be substituted by less toxic Mg without reducing the photovoltaic efficiency of the Methyl-ammonium lead iodide perovskites, the microscopic contributions to the absorption coefficients and efficiencies are analyzed as a function of the gradual substitution of Pb by Mg. The absorption coefficients were obtained from first principles and used later to obtain efficiencies. To identify and quantify the most important contributions to the photovoltaic properties as a function of cell thickness, both the absorption coefficients and efficiencies are split as an exact many-species expansion. From these results, the substitution of Pb by Mn would lead to solar cells with similar photovoltaics characteristics, except if the solar cells are ultra-thin.

Keywords: Perovskites; Optical properties; Photovoltaic; Semiconductors.

1. Introduction

Perovskite solar cells have undergone rapid progress as a result of their numerous advantages including low density, flexibility, and low cost-effective production. This great success mainly arises from the excellent optoelectronic properties with a high optical absorption coefficient, tunable band gap, long carrier recombination lifetime, and high electron/hole mobility. However, despite the progress in lead-halide perovskite solar cells, the commercialization still requires changing various aspects related to stability upon prolonged exposure to light, humidity, and high temperature. In addition, the perovskite solar cells with larger efficiency contain the toxic element lead. Toxic elements are a serious problem in many developing and industrializing countries. This is an impediment for future commercial development.

Therefore, it is important to know whether lead can be substituted for less toxic elements without reducing the efficiency. Nevertheless, the alternatives to lead must fulfill some criteria: (i) to maintain or even exceed the efficiencies. To achieve this, it is necessary that the alternatives have high absorption coefficients within the energy range of the solar spectrum; (ii) the new compounds should be stable; (iii) they should be low-cost, using abundant elements, and be easily recycled.

Metal halide perovskite materials have mainly the ABX_3 structure where A^+ represents an organic cation (for example, methyl ammonium $MA \equiv [CH_3NH_3]^+$), inorganic, or their mixture cation. B^{2+} is a smaller cation (Pb^{2+}, Sn^{2+} or Ge^{2+}) and X^- is a halide anion. Each B atom is coordinated by six X atoms that form an $[BX_6]^-$ octahedral framework, and each A is located at the center of the octahedral framework.

One of the most efficient solar cells has been obtained from $(MA)PbI_3$ (MAPI). According to the structure and the oxidation state, the best alternative would be to replace Pb with elements of the same group in the periodic table that admit the oxidation state +2, such as Sn and Ge, with similar outer shell *orbitals*. However, Pb-iodine perovskite is more stable than Sn-iodine perovskite [1]. The Sn in the perovskite easily undergoes the transformation from Sn^{2+} to Sn^{4+} reducing the photovoltaic efficiency [1,2]. In addition, Ge in perovskite is highly unstable in the divalent oxidation state [1,2]. Non-toxic alkaline earth metals Be, Mg, Ca, Sr, and Ba are abundant elements and have a stable divalent oxidation state. For this reason, these elements are considered good candidates for the replacement of toxic Pb. Some studies have focused on research of the energy band structure by doping the perovskite with Ca [3], Sr [4], and Ba [5]. Other alternatives for the replacement of Pb based on atoms that admit the oxidation state +2 have been proposed [6]: V, Mn, Ni, Cd, Hg, Ga, and In.

The band gap of $(MA)MgI_3$ is between 1.39 eV [7] and 1.50 eV [6], close to the band gap of $(MA)PbI_3$ (1.55 eV [8]), and close to the optimum one for photovoltaic performance (~1.3 eV for a sunlight spectrum with the maximum concentration) [9–11]). As a consequence, Mg [6] and the gradual substitution of Pb by Mg [7], i.e. $(MA)Pb_{1-x}Mg_xI_3$, have been identified as potential candidates for the total or partial replacement of Pb in organic-inorganic lead-halide perovskites [6,7]. However, only some experimental studies of Mg doping into perovskite were reported [7]. They showed that the efficiency was improved from 14.2 % to 17.8 % by increasing Mg doping from 0 to 1.0 %. Furthermore,

90% of the efficiency was still retained after storage in 30~40% relative humidity of 30 40% for 600 h. Therefore, research on how the gradual substitution of Pb by Mg affects the absorption coefficients and, as a consequence, the photovoltaic solar cell efficiency will be challenging and meaningful. Of course, even though Mg has been identified as a potential candidate for partial replacement of Pb [6] using a screening process based on the stability criteria, a more detailed analysis of the structural properties and stability of $(MA)Pb_{1-x}Mg_xI_3$ for all x would should be performed separately. For this, the $(MA)Pb_{1-x}Mg_xI_3$ enthalpy of formation should be compared with the corresponding values of any other combination of the elements into different compounds to check if $(MA)Pb_{1-x}Mg_xI_3$ formation results energetically favorable. Such a thorough analysis is beyond the scope of the current study.

One of the most important properties of materials that determine the absorption of solar radiation for subsequent conversion into useful energy is the absorption coefficient. In addition, knowledge of how the different atomic species of material influence the absorption coefficients will be very useful to analyze the most convenient substitutions without degrading the absorption coefficients. Note that partial or total substitution of Pb by other metal cations will modify the optoelectronic properties of perovskite materials. We will use first principles to calculate the absorption coefficients. Additionally, they will split into atomic contributions [12,13]. It permits to identify and quantify the most important contributions as a function of the photon energy. Using the absorption coefficients, the main parameters of the solar cell (current, voltage, and efficiency) can be quantified as a function of cell thickness. Furthermore, with the absorption coefficient splitting, the current and efficiencies can also be split [14]. It is described in the methodology section. Later, the results are presented and compared with other theoretical and experimental results. Finally, the main conclusions of this work are presented.

2. Results and discussion

2.1 Electronic structure

The experimental bandgaps reported in the literature for $(MA)Pb_{1-x}Mg_xI_3$ are between 1.61 eV [15] -1.63 eV [16,17] for x=0, i.e. $(MA)PbI_3$. The theoretically calculated bandgaps are between 0.98-1.69 eV (1.43 [18], 1.67 [15] 0.98-1.69 [19]) for x=0, i.e. $(MA)PbI_3$, and between 1.39 eV [7] and 1.50 eV [6] for x=1, i.e. $(MA)MgI_3$. The bandgaps

obtained in this work are 1.60 [6] eV and 1.40 eV for x=0 and 1 respectively. These calculated bandgaps are in general in good agreement with the experimental and theoretical values reported [6,8].

From the projected density of states (PDOS), for both crystalline structures, the valence band (VB) edge states came mainly from the p(I) orbitals, and the conduction band (CB) states predominantly from p(Pb) and s(Mg) with a smaller contribution from the p(I) orbitals. It is in agreement with other references in the literature [18,20–23]. Therefore, for energies close to the bandgap, the electronic properties are a consequence of the BI_6 (B=Pb, Mg) electronic interactions. As the organic cation states lie deep in the VB and CB, their contribution to the bandgap edge states is very small.

In many cases, the PDOS or Joint-DOS (JDOS) are used to carry out an analysis of the contributions to the optical properties. However, these analyses are appropriate for understanding electronic structures but inappropriate for analyzing photoexcitation properties, since transition probabilities are ignored. The property that determines the absorption capacity is the absorption coefficient. However, the absorption coefficient also does not provide any information on the contribution of the different species. For this reason, to explore the relationship of optical properties with the crystalline and atomic structure, the absorption coefficient has been split into interspecies contributions according to the methodological section.

2.2 Absorption coefficients

The $(MA)Pb_{1-x}Mg_xI_3$ total absorption coefficient α_T as well as the most important inter- (α_{AB}) and intra-atomic (α_{AA}) contributions, are shown in **Figure 1** for various x values. In this figure, α_{AA} and α_{AB} are terms of one and two species. The 3 and 4 species term (A_{34}) is also represented in the figure due to its importance. The $(MA)Pb_{1-x}Mg_xI_3$ have 6 species (5 for x = 0 and 1). Then the A_{34} term contains a high number of interactions of 3 and 4 species with a magnitude comparable or larger than the inter- and intra-species terms for certain energies. In fact, A_{34} is one of the most important terms above 3.5 eV. It includes the contribution of the organic cation species to the absorption coefficient. Their contribution to the absorption coefficient via A_{34} term is for larger

energies than the bandgap because the electronic states of the organic cation atoms lie deep within the VB and CB, i.e. their energetic separation is larger than the bandgap.

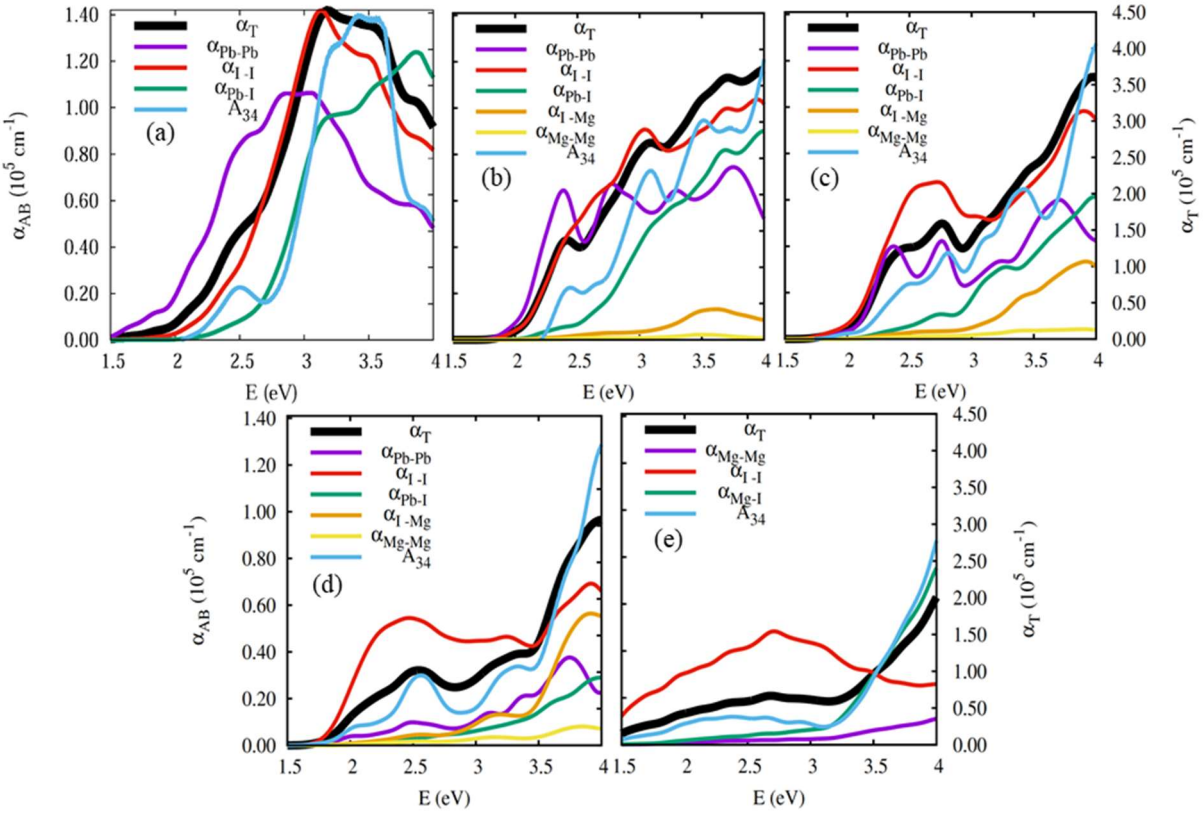

Figure 1. Total absorption coefficient α_T (right-hand *y* axis and thick black line) and the most important intra- and inter-species contributions α_{AB} (left-hand *y* axis) for the $(MA)Pb_{1-x}Mg_xI_3$ with (a) x=0.00, (b) 0.25, (c) 0.50, (d) 0.75, and (d) 1.00.

The results in Figure 1 for *x*=0 ($(MA)PbI_3$) reproduce the experimental absorption bands between 2.5-2.7 eV [24] attributed to the inter-species Pb-Pb ($\alpha_{Pb\text{-}Pb}$) [25], and between 3.2-3.5 eV [24] from the I-I ($\alpha_{I\text{-}I}$), Pb-I ($\alpha_{Pb\text{-}I}$) and Pb-Pb ($\alpha_{Pb\text{-}Pb}$) species transition. Furthermore, the absorption coefficient α_T reproduces the drop of the experimental absorption band between 3.5 and 4 eV [24].

With an increase in the Mg concentration, i.e. with *x*, the magnitude of the absorption coefficient α_T decreases within the range of energy shown in the figure. Moreover the most important contributions ($\alpha_{Pb\text{-}Pb}$, $\alpha_{I\text{-}I}$, $\alpha_{Pb\text{-}I}$ and A_{34}) also decrease with *x*. It seems obvious for contributions that involve Pb since increasing *x* decreases the Pb proportion. However, this is not accompanied by a significant increase in the terms that involve Mg

($\alpha_{\text{Mg-Mg}}$ and $\alpha_{\text{Mg-I}}$). Therefore, the optical absorption is dominated by electronic interactions of the PbI_6 octahedral framework, while MgI_6 contributes very little. As a consequence, as *x* increases also decreases $\alpha_{\text{I-I}}$. Another different aspect is its contribution to the total absorption coefficient α_T ($\alpha_{\text{I-I}}/\alpha_T$ and $\alpha_{\text{Pb-Pb}}/\alpha_T$). As α_T decreases more than $\alpha_{\text{I-I}}$ with *x* (in average value within the energies range shown in Figure 1), the contribution of $\alpha_{\text{I-I}}$ to α_T ($\alpha_{\text{I-I}}/\alpha_T$) will increase even if $\alpha_{\text{I-I}}$ decreases. The decrease of the $\alpha_{\text{Pb-Pb}}$ contribution to α_T ($\alpha_{\text{Pb-Pb}}/\alpha_T$) with *x* is obvious: increasing *x* decreases the Pb concentration until it is zero for *x* = 1. However α_T decreases with *x* but is not zero because of the other contributions. Therefore, although $\alpha_{\text{I-I}}$ decreases with *x*, its contribution to α_T ($\alpha_{\text{I-I}}/\alpha_T$) increases with *x*. This will be reflected on the contributions to total efficiency, as will be discussed later.

In summary, the main effects of the increase in *x* with respect to the absorption coefficients are: (i) a slight decrease in energy for the absorption onset due to a slight drop in bandgap; (ii) a significant decrease of the total absorption coefficients and of most of the contributions in the energy range of the solar spectrum photons (up to 4 eV approximately). These two effects have opposite consequences on the efficiency of solar cells~~, as it will analyze later~~. The first (i) increases efficiency because the bandgap is slightly close to the optimal absorption bandgap (~ 1.3 eV [9–11]). The second (ii) increases the penetration depth of the photons ($\sim\alpha_T^{-1}$), making thicker solar cells necessary to absorb them. This is not essential for thick solar cells, but it can be important for thin solar cells.

2.3 Efficiencies

With the absorption coefficients and the solar radiation spectrum voltages, currents and efficiencies can be obtained [12–14]. Total efficiency is shown in **Figure 2** as a function of cell thickness *w* using the AM1.5G spectra [26]. All photovoltaic parameters (efficiency η_T, current, and voltage) increased with Mg doping for large cell thickness *w,* in agreement with the experimental values reported [7]. This is mainly due to a slight

decrease in the bandgap with the increase in Mg. As a consequence, the bandgap approaches the optimal bandgap (~ 1.3 eV).

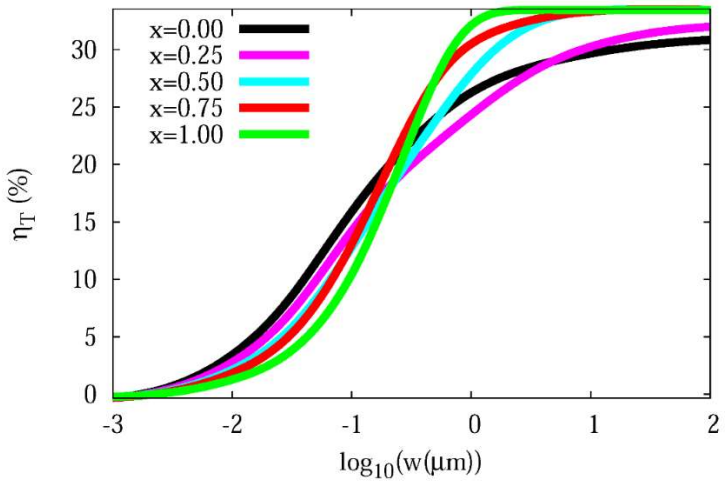

Figure 2. $(MA)Pb_{1-x}Mg_xI_3$ total efficiency η_T (%) as a function of the cell thickness *w* decimal logarithm using the AM1.5G spectra.

Moreover, much of the efficiency was still retained after storage in a humid environment for several hours [7]. However, for very thin solar cells, the efficiency decreases with *x*. This is because the magnitude of the absorption coefficients decreases with increasing *x,* as previously mentioned. As a consequence, the penetration depth (~ α_T^{-1}) increases with *x*. Therefore, fewer photons will be absorbed, thereby reducing the efficiency with increasing *x* for very thin solar cells.

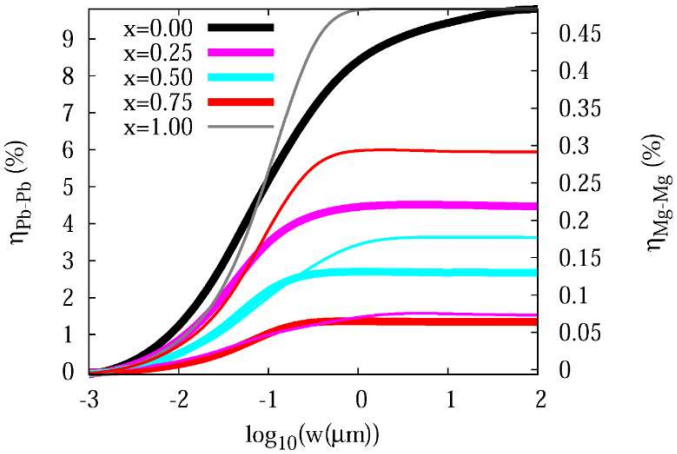

Figure 3. Same legend as that in Fig. 2, but for the $\eta_{Pb\text{-}Pb}$ (left-hand *y* axis and thick curves) and $\eta_{Mg\text{-}Mg}$ (right-hand *y* axis and thin curves) intra-specie contribution to the efficiency.

As mentioned above, a separation of the absorption coefficients in a sum of species contributions also allows splitting the efficiencies into an exact many-species expansion. The Pb-Pb ($\eta_{\text{Pb-Pb}}$) and Mg-Mg ($\eta_{\text{Mg-Mg}}$) intra-specie contributions to the $(MA)Pb_{1-x}Mg_xI_3$ efficiency are shown in the left-hand and right-hand *y* axis in **Figure 3**, respectively. Clearly the contribution $\eta_{\text{Pb-Pb}}$ decreases and that of $\eta_{\text{Mg-Mg}}$ increases with the increase of *x*. Similar to total efficiency η_T, split efficiencies decrease with decreasing thickness *w* as a result of lower absorption of photons.

The maximum magnitude of the scale on the left ($\eta_{\text{Pb-Pb}}$) and right ($\eta_{\text{Mg-Mg}}$) axes is very different. The corresponding to $\eta_{\text{Pb-Pb}}$ is much higher than that of $\eta_{\text{Mg-Mg}}$: 9.8 %, versus 0.48 % respectively. Therefore $\eta_{\text{Pb-Pb}}$ is much greater than $\eta_{\text{Mg-Mg}}$ even when the proportion of Mg is greater than that of Pb. For example, for $x = 0.75$ and large *w*, the Pb contribution to the efficiency is $\eta_{\text{Pb-Pb}} \sim 1.5$ % while that of Mg (in a higher proportion than Pb) is only $\eta_{\text{Mg-Mg}} \sim 0.3$ %. As $\eta_T \sim 34$ % (Figure 2), the Pb contributes ~ 4.4 % to η_T while Mg contributes only ~ 0.9 % to the total efficiency.

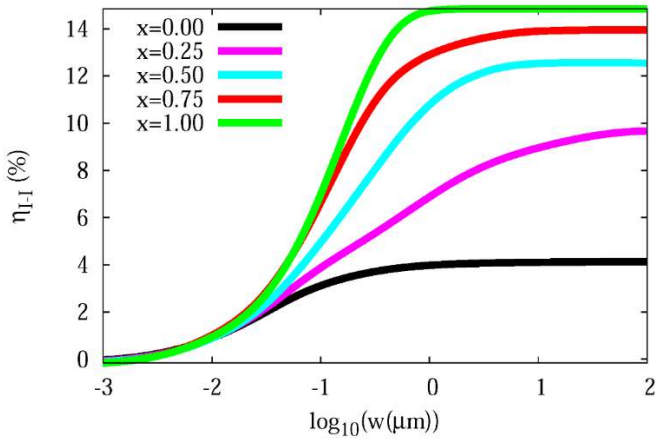

Figure 4. Same legend as that in Fig. 2, but for the $\eta_{I\text{-}I}$ intra-specie contribution to the efficiency.

However, as shown in Figure 2, for thick solar cells with large *w*, the efficiency η_T rises with increasing *x*. One of the reasons was already mentioned above: the bandgap slightly decreases approaching to the optimal bandgap. Another is the high $\eta_{I\text{-}I}$ contribution in all cases (**Figure 4**). This is a consequence of the effects of *x* on the

absorption coefficients mentioned above. Although $\alpha_{I\text{-}I}$ decreases with x (Figure 1), the total absorption coefficient α_T also decreases in the range of energies analyzed. However, as has been previously mentioned, the $\alpha_{I\text{-}I}$ contribution to α_T ($\alpha_{I\text{-}I}/\alpha_T$) increases with x. Similarly, the $\eta_{I\text{-}I}$ contribution to η_T (Figure 4) is very important and increases with x.

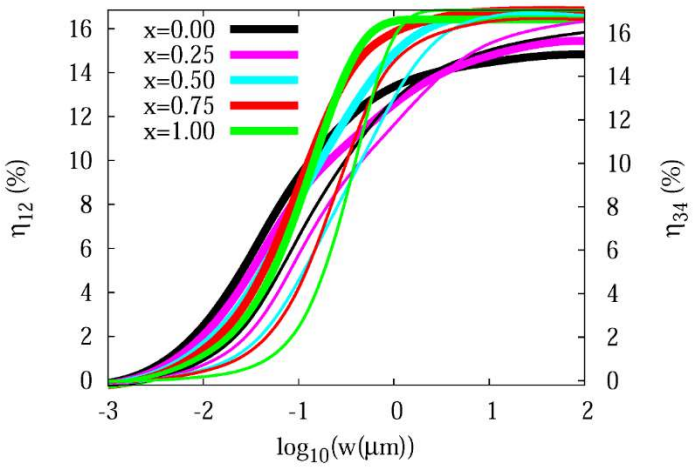

Figure 5. Same legend as that in Fig. 2, but for (a) the terms of one and two species A_{12} (left-hand y axis and thick curves), and three and four species contributions A_{34} (right-hand y axis and thin curves) to the efficiency.

Finally, the contribution to efficiency as a function of the thickness w of the sum of the terms of one and two species η_{12} (intra- and inter-species contributions) versus the sum of the terms of 3 and 4 species contributions η_{34} are shown in the left-hand and right-hand y axis respectively in **Figure 5**. $\eta_{12} = \sum_A \sum_B \eta_{AB}$ is obtained using the intra- and inter-species contributions to the absorption coefficients ($A_{12} = \sum_A \sum_B \alpha_{AB}$), and η_{34} using A_{34}. Note that $\alpha_T = A_{12} + A_{34}$ and $\eta_T = \eta_{12} + \eta_{34}$. The scale of the left-hand and right-hand *y-axes* is similar. Therefore, the η_{12} and η_{34} contributions to efficiency are similar. Furthermore, the contribution of both terms η_{12} and η_{34} for large w increases with x due to the slight decrease in the bandgap. However, for small x, the η_{12} contribution is larger than η_{34}. It is because for energies close to the bandgap $A_{12} \gg A_{34}$. A_{34} contributes significantly for energies larger than bandgap. Therefore, the photons absorbed by A_{34}

have a larger depth of penetration. They are only absorbed if the solar cell is thick, i.e. if *w* is large.

3. Conclusions

The electronic and optical properties of the $(MA)Pb_{1-x}Mg_xI_3$ mixed Pb-Mg perovskite compounds are obtained from first principles. From the absorption coefficients, the photovoltaic properties are also obtained. To quantify the microscopic contributions, we have split both the absorption coefficients and efficiencies into a many-species expansion. This splitting is exact, and there are no terms larger than those of 4 species.

The $(MA)Pb_{1-x}Mg_xI_3$ VB edge states come mainly from the p(I) orbitals, and the CB from p(Pb) and s(Mg) depending on *x,* and with a lesser contribution from the p(I) orbitals.

The absorption coefficients for energies close to the bandgap come mainly from the A_{12} term contributions. An *x* increase from 0 to 1 has two effects: (i) a slight reduction in the onset of absorption energy and (ii) a significant decrease in the total absorption coefficients. These two effects have opposite consequences on solar cell efficiency: (i) tends to increase efficiency mainly due to a slight decrease in the bandgap with the increase in Mg, and (ii) increases the photon penetration depth ($\sim\alpha_T^{-1}$) reducing efficiency for ultra-thin cells. Additionally, the $\alpha_{I\text{-}I}$ contribution to α_T is always very significant and increases with *x*. It is mainly a consequence of the $\alpha_{M\text{-}M}$ (M=Pb or Mg) reduction.

In any case, the substitution of Pb for Mn would lead to solar cells with similar photovoltaic characteristics, except if the solar cells are ultra-thin.

4. Methods

The electronic and optical properties are obtained using the density functional theory (DFT) [27] and a private modification of the SIESTA code [28]. The exchange-correlation potential is modelled by the generalized gradient approximation (GGA) from Perdew, Burke, and Ernzerhof [29] (PBE). To model the effect of the atomic inner electronic shells are used the Troullier–Martins [30] pseudopotentials expressed in the Kleinman–Bylander [31,32] form, and for the outer electron shell states a numerically localized pseudoatomic orbital basis set [33]. Generally, the use of a localized basis set combined with the GGA-PBE functional provides reasonable estimates of the bandgaps in organic-inorganic metal

halide perovskites [34]. It represents a compromise between accuracy and computational cost. In many cases a localized basis set is able to represent better the limited combination of states between the organic cation and the MI_6 (M=Pb, Mg) octahedron than a plane wave basis set for energies close to the bandgap [34]. On the other hand, the relativistic effects such as spin−orbit coupling, which is not considered here, would reduce the bandgap [35]. Therefore some more sophisticated methods with relativistic effects could compare worse despite being more accurate.

An analysis of the basis set has been carried out using from single-zeta to double-zeta with polarization basis sets for all atoms and varying the number of special k points in the irreducible Brillouin zone. In all the results presented, we use periodic boundary conditions with tetragonal structure supercell, double-zeta with polarization localized basis sets, and 72 k-point grids to sample the Brillouin zone. In the supercell Mg atoms have been substituted by Pb atoms, located as far as possible from each other.

The optical properties were obtained from the complex dielectric function using the Kramers-Kronig relationships [36]. We have developed a method [12,13] for calculating the contributions to the optical properties starting from first-principles calculations. With this methodology, the optical properties can be expressed as an exact many-species expansion [12,13] with terms that involve up to 4 species. For example, ~~for~~ the absorption coefficient can be expressed as $\alpha_T = \sum_\beta \alpha_\beta$ [12,13]. As a consequence, the efficiency can also be split as an exact many-species expansion ($\eta = \sum_\beta \eta_\beta$) [14]. To simplify the analyses, the absorption coefficients and efficiencies will be expressed as $\alpha_T = A_{12} + A_{34}$ and $\eta_T = \eta_{12} + \eta_{34}$ respectively. In both cases, the first term involves 1- and 2-species contributions: intra-species (A=B) and inter-species (A≠B) contributions ($A_{12} = \sum_A \sum_B \alpha_{AB}$ and $\eta_{12} = \sum_A \sum_B \eta_{AB}$). A_{34} and η_{34} involve 3-species (A≠B≠C) and 4-species (A≠B≠C≠D) contributions to the absorption coefficient and efficiency respectively.

Acknowledgments

This work has been supported by the National Spanish project MULTIPLER (RTI2018-096937-B-C21) and by the Comunidad de Madrid through the funding of the MADRID-PV2 (S2018/EMT-4308) project.

Conflict of Interest

The authors declare no conflict of interest.

List of references

[1] Q. Chen, N. D. Marco, Y. (Michael) Yang, T.-B. Song, C.-C. Chen, H. Zhao, Z. Hong, H. Zhou, Y. Yang, *Nano Today* **2015**, *10*, 355.
[2] P. P. Boix, K. Nonomura, N. Mathews, S. G. Mhaisalkar, *Mater. Today* **2014**, *17*, 16.
[3] C. Lu, J. Zhang, D. Hou, X. Gan, H. Sun, Z. Zeng, R. Chen, H. Tian, Q. Xiong, Y. Zhang, Y. Li, Y. Zhu, *Appl. Phys. Lett.* **2018**, *112*, 193901.
[4] D. Pérez-del-Rey, D. Forgács, E. M. Hutter, T. J. Savenije, D. Nordlund, P. Schulz, J. J. Berry, M. Sessolo, H. J. Bolink, *Adv. Mater.* **2016**, *28*, 9839.
[5] H. Zhang, M. Shang, X. Zheng, Z. Zeng, R. Chen, Y. Zhang, J. Zhang, Y. Zhu, *Electrochimica Acta* **2017**, *254*, 165.
[6] M. R. Filip, F. Giustino, *J. Phys. Chem. C* **2016**, *120*, 166.
[7] F. Yang, M. A. Kamarudin, G. Kapil, D. Hirotani, P. Zhang, C. H. Ng, T. Ma, S. Hayase, *ACS Appl. Mater. Interfaces* **2018**, *10*, 24543.
[8] M. A. Green, A. Ho-Baillie, H. J. Snaith, *Nat. Photonics* **2014**, *8*, 506.
[9] A. Luque, A. Martí, *Theoretical Limits of Photovoltaic Conversion, in Handbook of Photovoltaic Science and Engineering*, John Wiley & Sons Ltd, **2003**.
[10] P. Würfel, *Physics of Solar Cells. From Principles to New Concepts*, WILEY-VCH Verlag GmbH & Co, KGaA, **2005**.
[11] M. A. Green, *Third Generation Photovoltaics. Advanced Solar Energy Conversion*, Springer-Verlag Berlin Heidelberg, **2003**.
[12] C. T. Crespo, *Sol. Energy Mater. Sol. Cells* **2019**, *195*, 269.
[13] C. T. Crespo, *Sol. Energy Mater. Sol. Cells* **2019**, *200*, 110022.
[14] C. T. Crespo, *J. Phys. Chem. C* **2020**, *124*, 12305.
[15] C. Quarti, E. Mosconi, J. M. Ball, V. D'Innocenzo, C. Tao, S. Pathak, H. J. Snaith, A. Petrozza, F. De Angelis, *Energy Env. Sci* **2016**, *9*, 155.
[16] Y. Kawamura, H. Mashiyama, K. Hasebe, *J. Phys. Soc. Jpn.* **2002**, *71*, 1694.
[17] A. Maalej, Y. Abid, A. Kallel, A. Daoud, A. Lautié, F. Romain, *Solid State Commun.* **1997**, *103*, 279.
[18] T. Baikie, Y. Fang, J. M. Kadro, M. Schreyer, F. Wei, S. G. Mhaisalkar, M. Graetzel, T. J. White, *J Mater Chem A* **2013**, *1*, 5628.
[19] J. Feng, B. Xiao, *J. Phys. Chem. Lett.* **2014**, *5*, 1278.
[20] C. Grote, B. Ehrlich, R. F. Berger, *Phys Rev B* **2014**, *90*, 205202.
[21] E. Mosconi, A. Amat, Md. K. Nazeeruddin, M. Grätzel, F. De Angelis, *J. Phys. Chem. C* **2013**, *117*, 13902.
[22] S. X. Tao, X. Cao, P. A. Bobbert, *Sci. Rep.* **2017**, *7*, 14386.
[23] Y. D. Zhang, J. Feng, *AIP Adv.* **2018**, *8*, 015218.
[24] N. Kitazawa, Y. Watanabe, Y. Nakamura, *J. Mater. Sci.* **2002**, *37*, 3585.
[25] M. Hirasawa, T. Ishihara, T. Goto, *J. Phys. Soc. Jpn.* **1994**, *63*, 3870.
[26] *Http://Rredc.Nrel.Gov/Solar/Spectra/Am1.5/ASTMG173/ASTMG173.Html*, **n.d.**
[27] W. Kohn, L. J. Sham, *Phys Rev* **1965**, *140*, A1133.
[28] J. M. Soler, E. Artacho, J. D. Gale, A. García, J. Junquera, P. Ordejón, Daniel Sánchez-Portal, *J. Phys. Condens. Matter* **2002**, *14*, 2745.
[29] J. P. Perdew, K. Burke, M. Ernzerhof, *Phys Rev Lett* **1996**, *77*, 3865.

[30] N. Troullier, J. L. Martins, *Phys Rev B* **1991**, *43*, 1993.
[31] L. Kleinman, D. M. Bylander, *Phys Rev Lett* **1982**, *48*, 1425.
[32] D. M. Bylander, L. Kleinman, *Phys Rev B* **1990**, *41*, 907.
[33] O. F. Sankey, D. J. Niklewski, *Phys. Rev. B* **1989**, *40*, 3979.
[34] N. Hernández-Haro, J. Ortega-Castro, Y. B. Martynov, R. G. Nazmitdinov, A. Frontera, *Chem. Phys.* **2019**, *516*, 225.
[35] J. Even, L. Pedesseau, J.-M. Jancu, C. Katan, *J. Phys. Chem. Lett.* **2013**, *4*, 2999.
[36] G. F. Bassani, *Electronic States and Optical Transitions in Solids*, Pergamon Press, Oxford,New York, **1975**.

Table of contents entry

César Tablero Crespo

Effect of Substitution of Pb for Mg on the Photovoltaic Properties of Methyl-ammonium Lead Iodide Perovskites

The Methyl-ammonium Lead Iodide Perovskite, an absorber material for achieving low-cost high-efficiency photovoltaics, contains the toxic element lead. An attractive strategy is to replace Pb with Mg. In this work, this possibility is analyzed by carrying out a splitting of the most important contributions to the absorption coefficients and efficiencies.